Using Modified Empirical Mode Decomposition for Iris Recognition

Ming-Yu Huang¹, Jen-Chun Lee¹, Chien-Ping Chang¹, Ping S. Huang² and Te-Ming Tu¹

¹Department of Electrical and Electronic Engineering, Chung Cheng Institute of Technology,
National Defense University

²Department of Electronic Engineering, Ming Chuan University

ABSTRACT

As the demand of information security increases, so does the attention paid to the biometrics-based, automated person identification. Among current biometric approaches, iris recognition is known for an inherently reliable technique to identify one's identity. Empirical Mode Decomposition (EMD), a multi-resolution decomposition technique, is adaptive for non-linear and non-stationary data analysis, and therefore would be suitable for iris pattern extraction. This paper presents an effective approach for iris recognition using the proposed scheme of Modified Empirical Mode Decomposition to analyze the iris signals locally. Based on EMD that is a fully data-driven method and does not use any pre-determined filter or wavelet function, an iris recognition scheme is presented by adopting Modified EMD as a low-pass filter for feature extraction. To evaluate the proposed approach, three different similarity measures are used. Experimental results show that those three metrics have achieved promising and similar performance. Therefore, the proposed method demonstrates to be feasible for iris recognition and Modified EMD is suitable for feature extraction.

Keywords: biometrics, iris recognition, empirical mode decomposition (EMD), multi-resolution decomposition.

運用修改的經驗模態分解於虹膜識別

黄敏昱1 李仁軍1 張劍平1 黄炳森2 杜德銘1

¹ 國防大學理工學院電機電子工程研究所 ² 銘傳大學電子系

摘 要

隨著資訊安全需求資加,越來越多安全機制傾向於運用生物認證於人類身分認證,而現在生物認證的方法中,虹膜識別是一種非常可靠技術。經驗模態分解法(Empirical Mode Decomposition, EMD)是一種多解析分析技術,非常適合非線性及非穩態的資料分析,它分析訊號的局部性以及分離剩餘的訊號並擷取出高頻的訊號。基於經驗模態分解法是一種完全靠本身訊號而獲取所需資料的方法,不需任何前置處理過濾器或者小波等功能,本篇論文因此運用修改的經驗模態分解法為一低通濾波器分析虹膜影像後實施虹膜識別。提出的方法運用三種相似度量測方法評估,實驗證明三種相似度量測方法均達到卓越及相似的識別率,也顯示出修改的經驗模態分解法適合運用於虹膜識別。

關鍵詞:生物認證,虹膜識別,經驗模態分解,多解析分析

文稿收件日期 97.4.28.; 文稿修正後接受日期 97.9.19.

Manuscript received April 28, 2008; revised September 19, 2008.

I. INTRODUCTION

Biometrics is inherently a more reliable and capable technique to identity one's identity by his or her own physiological or behavioral characteristics. The features used for personnel identification by current biometric applications include facial features, fingerprints, iris, palm-prints, retina, handwriting signature, DNA, gait, etc. The comparison among those techniques were given in [1,2]. The lower error recognition rate achieved by iris recognition has been reported [3] and received increasing attention in recent years.

The eye appearance consists of sclera, iris, and pupil, and their boundaries are like circles with varied radii. Sclera is the outside portion of the eye occupying about 30% eye area. The central part of the eye is the pupil including 5% area of the eye. Iris is the colored portion of the exterior eye, which is embedded with tiny muscles that affect the pupil size, about 65% area of the eye [2], and is an annular part between the black pupil and white sclera. It appears that phenotypic random patterns are visible in the human iris constituted of lots of irregular blobs, such as freckles, coronas, stripes, furrows, crypts, etc. Such iris pattern is a unique, stable, and non-invasive biometric feature suitable for individual verification.

Nowadays, iris recognition approaches can be roughly divided into four methods: phase-based approaches [4-8], zero-crossing representation [9, 10], texture analysis [11-14], and intensity variation analysis [15,16]. Daugman's algorithm [4] adopted the 2D Gabor filters to demodulate the iris phase information. Each phase structure is quantized into one of four quadrants in the complex plane. The Hamming distance was further used to calculate the distance between iris codes of 2048 bits. In the past decade, Daugman had modified and improved his recognition algorithms [5-7]. A recent paper [8] presents alternative methods of segmentation based on active contours, a way to transform an off-angle iris image into a more frontal view, and a description of new score normalization scheme to use when computing Hamming distance that would account for the total amount of unmasked data available in the comparison. Boles and Boashash [9] presented the zero-crossing of one-dimensional wavelet transform to represent distinct levels of a concentric circle for an iris image, and then two dissimilarity functions were used for matching the obtained iris features. To

extend the approach of Boles and Boashash, Sanchez-Avila and Sanchez-Rellio [10] further proposed using different distance measures (such as Euclidean distance and Hamming distance) for feature matching. Wildes et al. [11] used the Laplacian pyramids to analyze the iris texture and combine features from four different resolutions. Then normalized correlation was selected to decide whether the input image and the enrolled image belong to the same class. Lim et al. [12] decomposed an iris image into four levels with different frequency components using two-dimensional Haar wavelet transform and the fourth-level with high frequency information was quantized to form an 87-bit code. Then a modified competitive learning neural network (LVQ) was used for classification. L. Ma et al. [13] proposed a well-known texture analysis method (multi-channel Gabor filtering) to capture both global and local details from an iris image. Recently, Tisse et al. [14] constructed the analytic image (a combination of the original image and its Hilbert transform) to demodulate the iris texture. L. Ma et al. proposed a local intensity variation analysis-based method and adopted the Gaussian-Hermite moments [15] and dyadic wavelet [16] to characterize the iris image for recognition.

Feature extraction is a crucial processing stage for pattern recognition [17]. Traditionally, basis techniques decomposition such as Fourier decomposition or Wavelet decomposition are selected to analyze real world signals [18]. Also, Fourier and Wavelet descriptors have long been used as powerful tools for feature extraction [19-21]. However, the main drawback of those approaches is that the basis functions are fixed, and do not necessarily match varying nature of signals. The Empirical Mode Decomposition (EMD) was firstly proposed by Huang et al. [22], with which any complicated data set can be decomposed into a finite and often small number of intrinsic mode function (IMF) components, which become the basis representing the data. Those extracted components can match the signal itself very well. Motivated by that EMD provides a decomposition method to analyze the signal locally and separate the component holding locally the highest frequency from the rest into a separate IMF. In this paper, we modified the EMD technique to extract the feature of the iris images for two reasons. The first reason is that modified EMD is a fully data driven method and does not use any pre-determined filter [15], wavelet function [16] or Fourier-wavelet basis [23]. For the second reason, it can easily be implemented and reduce the feature extraction and matching time. Therefore, here the modified EMD approach is used to extract residual components of the iris image as the feature for recognition.

This paper is organized as follows. Section 2 introduces preprocessing procedures for iris images. Section 3 and Section 4 describe the details of our proposed approach for feature extraction and matching. The experimental results are described and discussed in Section 5, prior to Conclusions in Section 6

II. IRIS IMAGE PREPROCESSING

The images of Human eye contain sclera, iris, pupil, eyelids, eyelashes and some skin outside the eye. To ensure that correct iris features can be easily extracted from the eye image, it is essential to perform preprocessing on the eye images. In this paper, we regard the human iris as an annular portion between the pupil (inner boundary) and the sclera (outer boundary). The image preprocessing procedures to extract the iris from the eye image are operated by three steps. The first is to locate the iris area. Then, the located iris is normalized and converted to a rectangular window of a fixed size in order to achieve the approximate scale invariance. Finally, illumination and contrast problems are eliminated from the normalized image through image enhancement, and the most irrelevant parts (such as eyelid, pupil, and eyelashes) are removed from the normalized image as much as possible by selecting an appropriate region of interest (ROI).

The iris image preprocessing procedures utilized in this paper is well described in the work [24, 25]. Generally speaking, we used only triad of points for locating the inner and outer boundaries of iris based on the Thales' theorem. The method does not need to find all the points on the inner and outer iris boundaries. Therefore, the computation process is efficient. The normalization process involves unwrapping the iris and converting it into its equivalent polar coordinates. We transform the circular iris area into a block with using Daugman's Rubber sheet model [5, 6]. The pupil center is considered the reference point and a remapping formula is used to convert the points from the

Cartesian scale to the polar scale. In our experiment, the radial resolution and the angular resolution are set to 64 and 512 pixels, respectively. After the normalization, iris templates would still have the problems of low contrast and non-uniform illumination. Here, the method proposed by L. Ma et al. [15] is adopted to eliminate the background brightness. Figure 1 illustrates the results of the preprocessing process for the iris image.

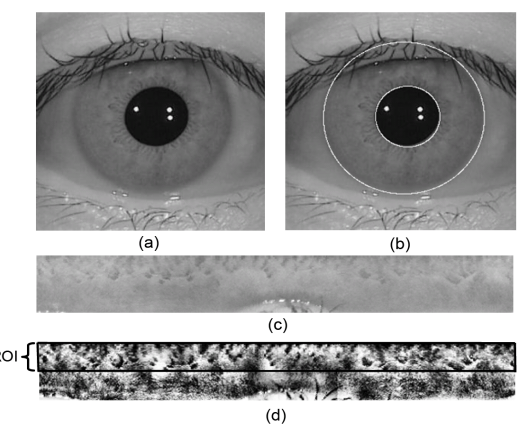


Fig. 1. The results of the iris image preprocessing (a) the original iris image, (b) the image with iris area located, (c) the normalized iris image, and (d) the ROI from the enhanced image.

III. FEATURE EXTRACTION

Despite all normalized iris templates have the same size and uniform illumination, there would be eyelashes and eyelids on the templates and those will bring down the performance of iris recognition. Therefore, the ROI is selected to remove the influence of eyelashes and eyelids that are shown in Fig. 1(d). The features are extracted only from the upper half region (32×512) close to the pupil that can provide the most discriminating information [26]. Doing this way can eliminate most of the interferences and produce more precise iris templates for feature extraction.

3.1 Empirical Mode Decomposition

The joint space-spatial frequency representations have received special attention in the fields of image processing, vision, and pattern recognition. Huang *et al.* [22] introduces a multi-resolution decomposition technique: the Empirical Mode Decomposition (EMD), which is

adaptive and appears to be suitable for non-linear, non-stationary signal processing method. The EMD method was originally proposed for the study of ocean waves [22], and found potential applications in geophysical exploration, underwater acoustic signals, noise removal filter and biomedicine *etc.* [28, 29]. The major advantage of EMD is that the basis functions are derived directly from the signal itself. Hence, the analysis is adaptive while compared with Fourier analysis, where the basis functions are linear combinations of fixed sinusoids.

Huang's solution [22] is to find a mean envelope by creating maximum and minimum envelopes around the signal using cubic spline interpolation through the respective local extrema. It can be argued that repeated iterations using cubic splines in EMD cause the loss of amplitude and frequency information [30]. In this paper, the technique of Modified EMD is proposed to improve EMD for iris feature extraction. The local mean of a signal is accomplished by progressively smoothing the signal using moving averaging. This averaging is weighted using the distance between the successive extrema of the signal by the following scheme. By considering the sample portion of iris data shown in Fig. 2, the local mean involves calculating the mean of the maximum and minimum points of half-wave oscillation of the signal. So the *i*th mean value m_i of each two successive extrema n_i and n_{i+1} is given by

$$m_i = \frac{n_i + n_{i+1}}{2} \tag{1}$$

In Fig. 2, local means can be plotted as straight blue lines computed from the mean of successive extrema. Those local means are then smoothed using moving averaging and displayed by a smoothly varying continuous local mean function m(t) (shown as the red line in Fig. 2).

The EMD principle is to decompose a signal into a sum of oscillatory functions, namely intrinsic mode functions (IMFs), that:

(a) an IMF has exactly one zero between any two consecutive local extremes.

(b) an IMF has a zero local mean.

The Modified EMD property is similar to EMD that a signal is decomposed into a sum of intrinsic mode functions (IMFs). The conditions satisfy the physically necessary conditions to define a meaningful instantaneous frequency. Otherwise, if

blindly applied to any analytic signal, instantaneous frequency may result in a few paradoxes [31, 32]: it may go beyond the band for bandlimited signal or it may not represent one of the frequencies in the Fourier spectrum in the global sense. So, the two conditions of an IMF allow the calculation of a meaningfully instantaneous frequency. Specifically, the first condition is similar to the narrow-band requirement, whereas the second condition modifies a global requirement to a local one by using the local mean of the envelopes defined by the local maxima and the local minima, and is necessary to certify that the instantaneous frequency will not have unnecessary fluctuations as induced by asymmetric waveforms. To make use of Modified EMD for practical applications, the signal must have at least two extrema-one maximum and one minimum to be successfully decomposed into IMFs. These IMF components are obtained from the signal by the means of an algorithm called sifting process. This algorithm extracts locally for each mode the highest frequency oscillations out of the original signal.

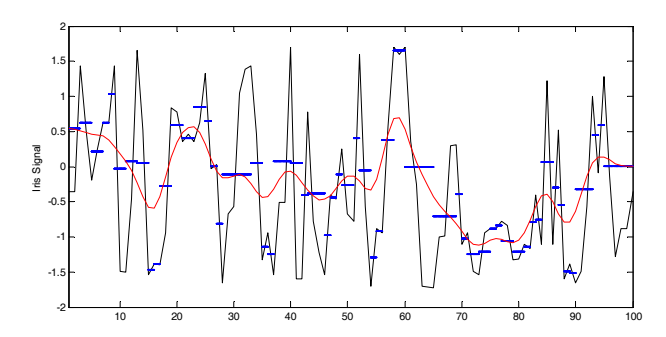


Fig. 2. Sample portion of iris data is displayed as the black line. The local means are shown by straight blue lines computed from the mean of successive extrema. The smoothed local mean is calculated by moving averaging and shown in red.

Given these two definitive requirements of an IMF, the sifting process for extracting IMFs from a given signal z(t), t=1,...,T is described as follows.

- 1) Identify all the maxima and minima of z(t).
- 2) Calculate the local mean of each two successive extrema using formula (1).
- 3) The local means are smoothed using moving averaging from a smoothly varying continuous local mean function m(t).

- 4) Extract the detail by d(t) = z(t) m(t).
- 5) Check the properties of d(t):
 - If d(t) meets the above-defined two conditions, an IMF is derived and replace z(t) with the residual r(t) = z(t) d(t);
 - If d(t) is not an IMF, replace z(t) with d(t).
- 6) Repeat Steps 1)–5) until the residual satisfies some stopping criteria.

At the end of this process, the original signal z(t) can then be reconstructed, using the following equation

$$z(t) = \sum_{i=1}^{n} c_i(t) + r_n(t)$$
 (2)

where n is the number of IMFs, $r_n(t)$ denotes the final residue which can be interpreted as the dc component of the signal, and $c_i(t)$ are nearly orthogonal to each other, and all have nearly zero means. Due to this iterative procedure, none of the sifted IMFs is derived in closed analytical form.

In fact, after a certain number of iterations, the resulting signals do not carry significant physical information, because, if sifting is carried on to an extreme, it could result in a pure frequency modulated signal of constant amplitude. To avoid this situation, we can stop the sifting process by limiting the normalized standard deviation (SD), computed from two consecutive sifting results. The SD is defined as

$$SD = \sum_{t=1}^{T} \frac{\left| z_{j}(t) - z_{j+1}(t) \right|^{2}}{z_{j}^{2}(t)}$$
 (3)

The SD is usually set between 0.2 and 0.3. By construction, the number of extrema is decreased when going from one residual to the next, and the whole decomposition is ensured to be completed with a finite number of modes. Figure 3 shows a simulated example of Modified EMD decomposition, where the analyzed signal (bottom left) is composed of an amplitude-modulated linear chirp (top left) and a triangular waveform (middle left). The Modified EMD, when applied to the signal, brings two IMF components and the final residual shown in Fig. 3 (right column). These two IMFs bear a striking similarity to the signals shown in Fig. 3 (left column). With the presence of the non-harmonic triangular waveform, any harmonic analysis such as Fourier

transform would end up with a much less compact and physically less meaningful decomposition [33].

By the nature of the decomposition procedure, the data is decomposed into n fundamental components, each with distinct time scale. More specifically, the first component associates with the smallest time scale which corresponds to the fastest time variation of data. As the decomposition process proceeds, the time scale increases, and hence, the mean frequency of the mode decreases. Based on this observation, we may devise a general purpose time-space filtering as

$$z_{lh}(t) = \sum_{i=1}^{h} c_i(t)$$
 (4)

where $l,h \in [1,...,n], l \le h$. For example, when l=1 and h < n, it is a high-pass filtered signal; when l > 1 and h = n, it is a low-pass filtered signal; when $1 < l \le h < n$, it is a band-pass filtered signal. The above equation forms the basis for our application of iris data described below, where we use it as a low-pass filtering.

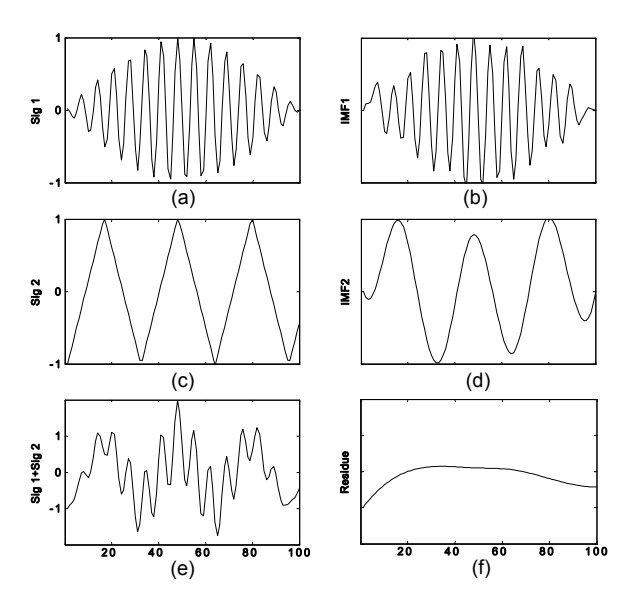


Fig. 3. A simulated example of Modified EMD Decomposition. Left column: (a) a amplitude-modulated linear chirp, (c) a triangular waveform, and (e) their composite signal. Right column: (b), (d) and (f) are two components (IMFs) and the last final residue extracted by Modified EMD revealing a striking agreement with the signals.

The Modified EMD algorithm extracts the oscillatory mode that exhibits the highest local

information from the data ("detail" in the wavelet context), leaving the remainder as a "residual" ("approximation" in wavelet analysis). According to the major advantage of Modified EMD that the process of deriving the basis functions is empirical, the basis functions are derived dynamically from the signal itself. As shown in Fig. 4, the sample iris images from [27], the irregular blocks of the iris are slightly darker than their surroundings. Therefore, it is reasonable to consider that the residual presents the basic characteristics of the iris and the detail denotes the variation of the noise represented by the highest local information. That is the motivation we use the Modified EMD as a low-pass filter and only the distinct iris characteristics are utilized as discriminating features for accurate iris recognition. The Modified EMD method yields six IMF components together with the final residual as shown in Fig. 5.



Fig. 4. Samples of iris images from CASIA.

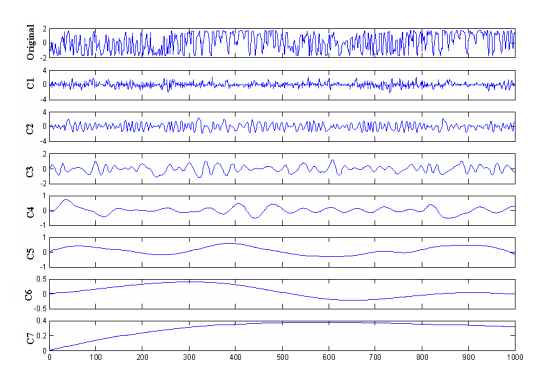


Fig. 5. Six IMF components and the residual (C7 on the bottom) of original iris signal obtained by Modified EMD method.

To illustrate how the Modified EMD can be used as a low-pass filter, we recover the iris original data from the IMF components. The step-by-step reconstruction is shown in Fig. 6 where the original data is plotted in blue lines and partial sum of the IMFs in red lines. The first plot shows the data and the last component C7, the residue of the sifting, which denotes the dc component in the data. The last

plot shows the summation of all the IMFs, which looks like the original data. The intermediate plots show the progress of addition of the IMF components. If we stopped at any step, the data was filtered.

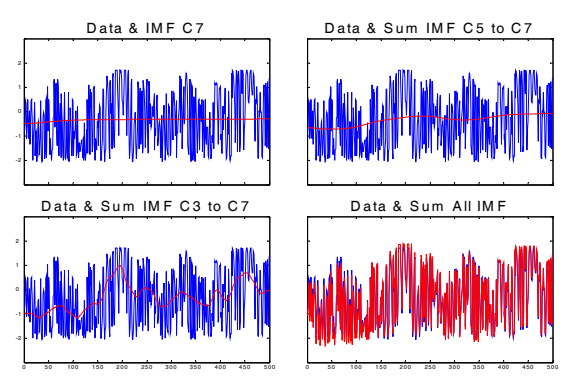


Fig. 6. Illustration of the Modified EMD acting as a low-pass filter through the reconstruction of the original iris data from the IMF components.

To associate with iris recognition, we also present the results of Modified EMD decomposition for iris images, as shown in Fig. 7. Note that the ROI of the normalized iris image is converted into a 1-D feature sequence by concatenating its rows. For easy comparison, Figure 7 shows only the first 500 components of their original feature sequences. Figure 7(a) and 7(c) shows the Modified EMD decomposition results of two iris images from the same person. Figure 7(b) and 7(d) demonstrates the Modified EMD results of two iris image from two different persons. To demonstrate the similarity of two iris images from the same person captured at different time, it is easily proved by checking those corresponding circles marked in Fig. 7(a) and 7(c). Also, those circles marked in Fig. 7(b) and 7(d) point out the differences of two iris images from two different persons.

3.2 Feature Vector

For the ROI of each normalized iris image I, pixel sequences from different rows are concatenated to form the 1-D vector V represented by

$$V = \{I_1 \cdots I_x \cdots I_K\} = \{v_1, v_2, \cdots v_i, \cdots, v_n\}$$
 (5)

where I_x denotes gray values of the xth row in the image I, v_i defines the pixel value of position

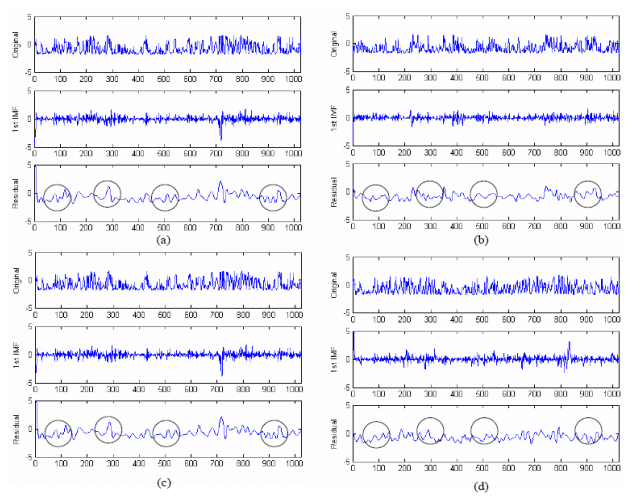


Fig. 7. (a) and (c) show the Modified EMD decomposition results of two iris images from the same person. (b) and (d) show the Modified EMD result of the iris image from two different persons.

j inside the vector V, and n is the number of total components, herein, $n=32\times512=16384$. After concatenation and before performing Modified EMD, the linear re-scaling [34] is applied to each vector to adjust the average of each data set to zero and to normalize the standard deviation to unity before further using the ROI vector. By calculating the mean \overline{v} and variance σ_v^2 with respect to the spatial template, the linear re-scaled V^N can be given by

$$V^{N} = \frac{V - \overline{v}}{\sigma_{v}} = \{v_{1}^{N}, v_{2}^{N}, \dots v_{j}^{N}, \dots, v_{n}^{N}\}$$
 (6)

where the mean $\overline{v} = \frac{1}{n} \sum_{j=1}^{n} v_j$, and the variance

$$\sigma_v^2 = \frac{1}{n-1} \sum_{j=1}^n (v_j - \overline{v})^2$$
. After Modified EMD

calculation, the feature vector of each Modified EMD residual from the 1-D vector \boldsymbol{V}^N can be obtained by

$$\mathbf{R}^{m} = \{R_{1}^{m}, R_{2}^{m}, \dots R_{i}^{m}, \dots, R_{n}^{m}\}$$
 (7)

where \mathbf{R}^m represents the *m*th residual of the Modified EMD results and R_j^m denotes the feature from the *j*th position of the R^m . In our experiments, the feature vector consists of 16384 components and the value of the *m* is one.

3.3 Invariance

Invariant to translation, scale, and rotation is a crucial factor while defining features to represent the iris images. In this article, an iris image is normalized to the polar coordinates and fixed to the same size to achieve the scale invariance. The translation invariance is associated with our algorithm to extract the feature from the original image. The rotation invariance can be achieved by shifting \mathbf{R}^m from the initial position of original 2D polar coordinates. Therefore, the feature vector \mathbf{R}^m is reshaped to 2D polar coordinates and circularly shifted. Due to that the size of \mathbf{R}^m is same as the 1-D vector V, hence, the shift value is set to -12, -8, -4, 0, 4, 8, 12, corresponding to rotating the original iris image by -9° , -6° , -3° , 0° , 3° , 6° , 9° , respectively. Thus, seven templates with seven rotation angles for each iris class are stored in the database. When the input feature vector is matched with the seven templates of a class, the minimum of the seven scores is taken as the final matching score.

IV. MATCHING

It is important to choose a suitable similarity measure between feature vectors. In this section, we discuss how to evaluate the performance of our proposed method. The main goal of iris recognition is to match the unknown iris feature with those known iris feature classes in the database and determine whether the unknown feature comes from the authentic one or the imposter. The matching process is to be made with the unknown feature, which will be calculated depending on different metrics. In this article, three different similarity measures used as the matching criterion are:

1)The mean of the Euclidean distances (MED) measure: This metric gives a measure of how similar a collection of values are between two classes. The MED measure is specified as

$$d_1(p,q) = \sqrt{\frac{1}{M} \sum_{i=1}^{M} (p_i - q_i)^2}$$
 (8)

where $M = K \times L$ is the dimension of the feature vector, p_i is the *i*th component of sample feature vector, and q_i is the *i*th component of unknown sample feature vector.

2) Cosine Similarity: The idea is that two vectors p,

q are more equal the closer they get i.e. the smaller the angle. A similar definition can be used in the vector space, whereby the cosine of the angle between two vectors is defined as

$$d_2(p,q) = 1 - \frac{p}{\|p\|} \frac{q}{\|q\|} \tag{9}$$

where p and q are two different feature vectors. $\| ullet \|$ indicates the Euclidean norm. The

range of $\frac{p}{\|p\|} \frac{q}{\|q\|}$ is [0,1]. The more similar the

two vectors are, the smaller the $d_2(p,q)$ value is.

3) Hamming distance: The *distance* of two sequences with equal length are calculated by counting the character positions in which they differ. This can be found by using XOR operation. The binary Hamming distance (HD) measure is defined as

$$d_3(p,q) = \frac{1}{M} \sum_{i=1}^{M} p_i \oplus q_i$$
 (10)

where \oplus denotes Exclusive-OR, M is the length of the binary sequence. p_i is the ith component of the database sample feature vector, and q_i is the ith component of the unknown sample feature vector. In our experiments, we designed that each component value of the feature vector is set to 1 while the value of the first residual in the iris Modified EMD signature is positive or null, otherwise 0.

V. EXPERIMENTAL RESULTS

This section describes the experimental results obtained from the experiments performed by using the proposed approach. In the verification mode, we can obtain the receiver operating characteristic (ROC) curve that depicts the relationship of false match rate (FMR) and false non-match rate (FNMR). The area under the ROC curve (denoted as Az) reflects how well the intra-class and inter-class distributions can be distinguished and the ranges are from 0.5 to 1. For an ideal ROC curve, the value of Az should be 1. It denotes that the intra- and inter-class are inseparable while the Az value is equal to 0.5. Hence, ROC curve is normally used to measure the accuracy of the matching process, showing the achieved

performance of an algorithm. Meanwhile, the equal error rate (EER) is also used for performance evaluation. In the recognition mode, the correct recognition rate (CRR) is adopted to assess the efficacy of the algorithm.

5.1 Iris Database

At present, most proposed methods for iris recognition used small data sets to evaluate their performance, and only the L. Ma et al. [13, 15, 16] and Daugman's approach [4-8] had been tested on a large image set involving over 200 subjects. In our experiments, the test data set is from the generally used iris image database, CASIA Iris Database [27], authorized from the Institute of Automation, Chinese Academy of Science. Each image has the resolution of 320×280 in 8-bit gray level. This database includes 1992 iris images from 249 different eyes (hence, 249 different classes) with 8 each. The images are acquired during different sessions and the time interval between two collections is at least one month. Three images of each class are selected randomly to constitute the training set and the remaining images of each class are treated as the test set. In the preprocessing stage, we checked the segmentation accuracy of the iris boundaries subjectively and obtained an accuracy rate of 95.9% (81 images are not used) on 1992 images. Table 1 shows different causes of the iris locating failure. Therefore, there are 747 images for training and 1164 images for testing. Using those 1911 different iris images from the CASIA Iris Database, the experiments conducted below are running on the computing environment of 1.8GHz PC with 736MB RAM using Matlab 6.5.

Table 1. Failure analysis of locating iris for different causes

Cause of Failure	Number of images (CASIA)
Occlusion by eyelids	31
Inappropriate eye positioning	21
Occlusion by eyelash	23
Noises within iris	6
Total	81

5.2 Performance Evaluation of the Proposed Method

To assess the accuracy of the proposed

algorithm, each iris test image in the database is compared with all the other iris test images in the database. In the CASIA iris database, the total test number of comparisons is 1,350,819, where the total test number of intra-class comparisons is 2,148 and that of inter-class comparisons is 1,348,671. Table 2 demonstrates promising recognition results achieved by our proposed method using three similarity measures from (8)-(10). Note that performance differences are not very significant while different similarity measures are used. Only a slightly higher recognition rate of 99.04% is accomplished by using the MED similarity measure in the identification tests. The verification results are shown in Figure 8. It displays the ROC curve accomplished by the proposed method under different similarity measures. The Az value (the area under the ROC curve) is up to 0.9996 by the MED similarity measure. Therefore, experimental results show that the proposed iris representation is effective and the Modified EMD approach can really extract the promising feature from each iris image.

Table 2 Recognition rates of three similarity measures achieved by Modified EMD with different threshold values

Similarity measure	Threshold	Correct recognition rate (CRR) %
MED	0.45	99.04
Cosine	0.38	98.78
HD	0.72	98.32

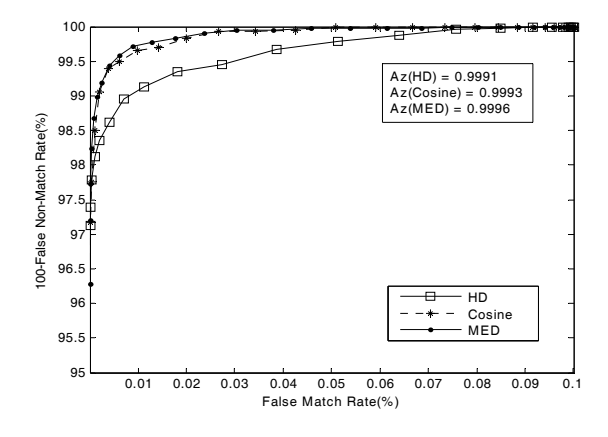


Fig. 8. The ROC curve of Modified EMD method with different similarity measures.

5.3 Boundary Processing for Modified EMD

The EMD firstly proposed by Huang et al. [22] is a method of breaking down a signal into a series of zero-mean AM-FM components by iteratively conducting the sifting process that we have introduced in Section 3.1. As pointed out by [22], "Serious problems of the spline fitting can occur near the end points, where the cubic spline can have large swings." Hence, we adopt the method introduced in [35] to eliminate the boundary effects and evaluate the recognition results to see if it can be improved in this experiment.

This simple boundary processing procedure is performed by the even extension and the odd extension. To construct a periodic signal from arbitrary time series is easily accomplished by the even extension. Near the end points, the outside of the original data is spanned by the mirror image of those inside. The odd extension also provides all advantages which the even extension does. While the fact that the mean of the even extension and the odd extension is same as the original data series inside the data span and zero outside the data span brings a simple boundary processing technique for EMD described in [35].

The verification results are shown in Table 3. Compared to the results in Table 2, only a slightly higher recognition rate is improved for the MED similarity measure and a slightly lower recognition rate is affected for the HD similarity measure. The experimental results achieved in the ROC curve and three operating states are the same as shown in Fig. 8. Table 4 shows the feature extraction time with and without considering the boundary condition. As displayed in Table 4, the computation time without considering the boundary condition is faster than that of with considering the boundary condition almost three times. Clearly, by using the Modified EMD technique, the iris recognition performance does not make apparent difference while considering the boundary effect.

Table 3 Recognition rates achieved while considering the boundary condition in Modified EMD with three similarity measures

similarity incustries		
Similarity measure	Correct recognition rate	
MED	99.22%	
Cosine	98.83%	
HD	98.17%	

Table 4 Feature extraction time with and without considering the boundary condition in Modified EMD

LIVID	
Ignoring	Considering
boundary(ms)	boundary(ms)
245	706

5.4. Comparison and Discussion

Experimental results from previous paragraphs reveal that the proposed technique is an effective scheme for feature extraction and the MED similarity measure can achieve a correct recognition rate up to 99.04%. To compare with the other iris recognition algorithms, we have also implemented two methods, the approaches of the Fourier-wavelet feature [23] and the Gaussian-Hermite moments [15]. Together with our proposed scheme, three approaches are tested using the 249 classes of the CASIA Iris Database and the cosine similarity measure. Table 5 and Fig. 9 demonstrate the experimental results. Table 5 illustrates that the Az accomplished by each algorithm is greater than 0.9 and the CRR exceeds 90% as well. This implies that the high accuracy can be achieved by those three methods. Although a slightly lower recognition rate than the approach of Gaussian-Hermite moments is achieved, the proposed method still can fulfill the demand of high accuracy suitable for very high security environments. Figure 9 displays the ROC curve of those three methods. From the results shown in Table 5 and Fig. 9, we can find that the method of Gaussian-Hermite moments achieves the best performance, followed by the proposed method, and then the method of Fourier-wavelet feature.

To evaluate the computation complexity, Table 6 shows the computational costs consumed by three methods with cosine similarity measure, including the CPU time for feature extraction and matching. Our proposed method using the Modified EMD

Table 5 Recognition rates achieved by different methods using the cosine similarity measure

Methods	CRR %	Az	EER (%)
Fourier-wavelet feature[23]	94.37	0.9888	5.24
Gaussian-Hermite moments[15]	99.21	≅ 1	0.48
Proposed method	99.04	0.9993	1.82

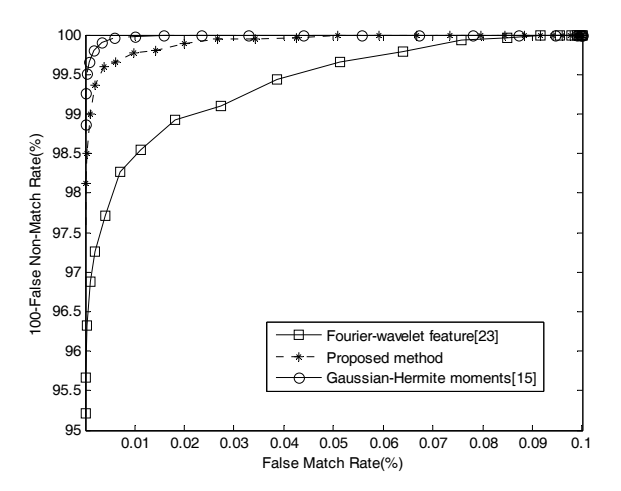


Fig. 9. The ROC curve of different methods using the cosine similarity measure.

Table 6 Comparison of the computational complexity

Methods	Feature extraction(ms)	Matching (ms)
Fourier-wavelet feature[23]	1297	76
Gaussian-Hermi te moments[15]	426	34
Proposed method	245	56

method for feature extraction demonstrates the best performance. This can be a potential advantage for iris matching in a large database.

Based on the previous experimental results with corresponding analysis, we can conclude:

- 1. The proposed method can achieve high accuracy and fast performance for iris recognition. This also indicates that the Modified EMD technique can extract discriminating features suitable for iris recognition.
- 2. Compared with the method of Gaussian-Hermite moments [15], our proposed method still needs to be improved in the performance. Therefore, feature selection is an important research issue in the near future.

VI. CONCLUSIONS

In this paper, a novel and effective method for iris recognition is presented, which operates using the Modified EMD technique. This paper also evaluates the effect of the boundary processing for

iris recognition. The performance of iris recognition achieved by the Modified EMD approach associated with three different similarity measures has been evaluated. Experimental results have shown that without taking account the boundary effect still can demonstrate eminent performance. The best metric is the MED measure and the other two measures also have achieved similar performance more than 95%. Therefore, the proposed method has demonstrated to be promising for iris recognition and Modified EMD is suitable for feature extraction. In the future, we will ameliorate the template processing method to reduce the influence of light, eyelid, and eyelash. We are also working at increasing the database in order to further verify the performance and trying other possible approaches to improve the classification accuracy.

REFERENCES

- [1] Jain, A. K., Bolle, R., and Pankanti, S., Biometrics: Personal Identification in Network Society, Kluwer Academic Publishers, 1999.
- [2] Miller, B., "Vital Signs of Identity," *IEEE Spectrum*, Vol. 31, pp. 22-30, 1994.
- [3] Mansfield, T., Kelly, G., Chandler, D., and Kane, J., "Biometric Product Testing Final Report," issue 1.0, National Physical Laboratory, March, 2001.
- [4] Daugman, J., "High Confidence Visual Recognition of Persons by a Test of Statistical Independence," IEEE Transactions on Pattern Analysis and Machine Intelligence, Vol. 15, No. 11, pp. 1148-1161, 1993.
- [5] Daugman, J., "Statistical Richness of Visual Phase Information: Update on Recognizing Persons by Iris Patterns," Int'l Journal on Computer Vision, Vol. 45, No. 1, pp. 25-38, 2001.
- [6] Daugman, J., "How Iris Recognition Works", IEEE Transactions on Circuits and Systems for Video Technology, Vol. 14, No. 1, pp. 21-30, 2004.
- [7] Daugman, J., "Probing the uniqueness and randomness of iriscodes: Results from 200 billioniris pair comparisons," Proceedings of the IEEE, Vol. 94, No. 11, pp. 1927–1935, 2006.
- [8] Daugman, J., "New methods in iris recognition," IEEE Transactions on Systems, Man and

- Cybernetics B, Vol. 37, No. 5, pp. 1167–1175, 2007.
- [9] Boles, W. W., and Boashash, B., "A Human Identification Technique Using Images of the Iris and Wavelet Transform", IEEE Transactions on Signal Processing, Vol. 46, No. 4, pp. 1185-1188, April, 1998.
- [10] Sanchez-Avila, C., and Sanchez-Reillo, R., "Iris-Based Biometric Recognition Using Dyadic Wavelet Transform," IEEE Aerospace and Electronic Systems Magazine, Vol. 17, No. 10, pp. 3-6, 2002.
- [11] Wildes, R., Asmuth, J., Green, G., Hsu, S., Kolczynski, R., Matey, J., and McBride, S., "A Machine-Vision System for Iris Recognition," Machine Vision and Applications, Vol. 9, No. 1, pp. 1-8, 1996.
- [12] Lim, S., Lee, K., Byeon, O., and Kim, T., "Efficient Iris Recognition through Improvement of Feature Vector and Classifier," ETRI J., Vol. 23, No. 2, pp. 61-70, 2001.
- [13] Ma, L., Tan, T., Wang, Y., and Zhang, D., "Personal Identification Based on Iris Texture Analysis," IEEE Transactions on Pattern Analysis and Machine Intelligence, Vol. 25, No. 12, pp.1519-1533, 2003.
- [14] Tisse, C., Martin, L., Torres, L., and Robert, M., "Person Identification Technique Using Human Iris Recognition," Journal of System Research, Vol. 4, pp.67-75, 2003.
- [15] Ma, L., Tan, T., Wang, Y., and Zhang, D., "Local Intensity Variation Analysis for Iris Recognition," Pattern Recognition, Vol. 37, pp.1287-1298, 2004.
- [16] Ma, L., Tan, T., Wang, Y., and Zhang, D., "Efficient Iris Recognition by Characterizing Key Local Variations", IEEE Transactions on Image Processing, Vol. 13, No. 6, pp. 739-750, June, 2004.
- [17] Trier, O. D., Jain, A. K., and Taxt, T., "Feature Extraction Methods for Character Recognition A Survey," Pattern Recognition, Vol. 29, pp. 641-662, 1996.
- [18] Daubechies, I., Ten Lectures on Wavelets, SIAM, Philadelphia, Pennsylvania, 1992.
- [19] Wang, S. S., Chen, P. C., and Lin, W. G., "Invariant Pattern Recognition by Moment Fourier descriptor," Pattern Recognition, Vol. 27, pp. 1735-1742, 1994.
- [20] Granlund, G. H., "Fourier Processing for

- Handwritten Character Recognition," IEEE Transactions on Computer, Vol. 21, pp. 195-201, 1992.
- [21] Wunsch, P., Laine, A. F., "Wavelet Descriptors for Multiresolution Recognition of Handprinted Characters," Pattern Recognition, Vol. 28, pp. 1237-1249, 1995.
- [22] Huang, N., Shen, Z., Long, S., Wu, M., Shih, H., Zheng Q., Yen N., Tung C., and Liu H., "The Empirical Mode Decomposition and Hilbert Spectrum for Nonlinear and Non-stationary Time Series Analysis," Proc. of the Royal Society of London, Vol. 454, pp. 903–995, 1998.
- [23] Huang, P. S., Chiang, C. S., and Liang, J. R., "Iris Recognition Using Fourier-Wavelet Features", Lecture Notes in Computer Science (LNCS), Vol. 3546, pp. 14-22, 2005.
- [24] Lee, J. C., Huang, P. S., Chang, J. C., Chang, C. P. and Tu T. M., "Iris Recognition Using Local Texture Analysis," Optical Engineering, Vol. 47, No. 6, pp. 067205-1-067205-10, June, 2008.
- [25] Lee, J. C., Huang, P. S., Chang, J. C., Chang, C. P., and Tu, T. M., "Novel and Fast Approach for Iris Location," Proceedings of the Third International Conference on Intelligent Information Hiding and Multimedia Signal Processing(IIHMSP07), Vol. 1, pp.139-142, Nov. 2007. Kaohsiung, Taiwan.
- [26] Sung, H., Lim, J., Park, J., and Lee, Y., "Iris Recognition Using Collarette Boundary Localization," in the Proceedings of the 17th International Conference on Pattern Recognition, Vol. 4, pp. 857-860, Aug. 2004.
- [27] Institute of Automation, Chinese Academy of Science, CASIA Iris Image Database. http://www.sinobiometrics.com/chinese/chinese.htm
- [28] Huang, W., Shen, Z., Huang, N. E., and Fung, Y. C., "Engineering analysis of biological variables: An example of blood pressure over 1 day," Proc.Nat. Acad. Sci. USA., Vol. 95, pp. 4816–4821, 1998.
- [29] Liang, H., Lin, Z., and McCallum, R. W., "Artifact reduction in electrogastrogram based on the empirical model decomposition method," Med. Biol. Eng. Computer., Vol. 38, pp. 35–41, 2000.
- [30] Huang, Y. P., Li, X. Y., and Zhang, R. B., "A Research on Local Mean in Empirical Mode

- Decomposition," Lecture Notes in Computer Science (LNCS), Vol. 4489, pp. 125-128, 2007.
- [31] Boashash, B., "Estimating and interpreting the instantaneous frequency of a signal-part I: Fundamentals," Proc. IEEE, Vol. 80, pp. 520–538, 1992.
- [32] Cohen, L., Time-Frequency Analysis. Englewood Cliffs, NJ: Prentice-Hall, 1995.
- [33] Rilling, G., Flandrin, P., and Goncalves, P., "On empirical mode decomposition and its algorithms," in Proc. IEEE-EURASIP Workshop on Nonlinear Signal and Image Processing, 2003.
- [34] Bishop, C. M., Neural Networks for Pattern Recognition, Oxford University Press, 1996.
- [35] Zeng, K., and He, M. X., "A Simple Boundary Process Technique for Empirical Mode Decomposition", in the Proceeding of IEEE International Symposium on Geoscience and Remote Sensing, IGARSS04. Vol. 6, pp. 4258-4261, 2004.